Tracking the completion of parts into whole objects: Retinotopic activation in response to illusory figures in the lateral occipital complex

Siyi Chen [a,*], Ralph Weidner [b], Hang Zeng [b], Gereon R. Fink [b,c], Hermann J. Müller [a], Markus Conci [a]

[a] Ludwig-Maximilians-Universität München, 80802, München, Germany
[b] Cognitive Neuroscience, Institute of Neuroscience and Medicine (INM-3), Research Center Jülich, 52428, Jülich, Germany
[c] Department of Neurology, University Hospital Cologne, Cologne University, 50937, Cologne, Germany

ARTICLE INFO

ABSTRACT

Illusory figures demonstrate the visual system's ability to integrate separate parts into coherent, whole objects. The present study was performed to track the neuronal object construction process in human observers, by incrementally manipulating the grouping strength within a given configuration until the emergence of a whole-object representation. Two tasks were employed: First, in the spatial localization task, object completion could facilitate performance and was task-relevant, whereas it was irrelevant in the second, luminance discrimination task. Concurrent functional magnetic resonance imaging (fMRI) used spatial localizers to locate brain regions representing task-critical illusory-figure parts to investigate whether the step-wise object construction process would modulate neural activity in these localized brain regions. The results revealed that both V1 and the lateral occipital complex (LOC, with sub-regions LO1 and LO2) were involved in Kanizsa figure processing. However, completion-specific activations were found predominantly in LOC, where neural activity exhibited a modulation in accord with the configuration's grouping strength, whether or not the configuration was relevant to performing the task at hand. Moreover, right LOC activations were confined to LO2 and responded primarily to surface and shape completions, whereas left LOC exhibited activations in both LO1 and LO2 and was related to encoding shape structures with more detail. Together, these results demonstrate that various grouping properties within a visual scene are integrated automatically in LOC, with sub-regions located in different hemispheres specializing in the component sub-processes that render completed objects.

1. Introduction

Organizing the retinal image into meaningful and coherent objects is a fundamental task of human vision. For example, as illustrated by the so-called 'Kanizsa' figure (Kanizsa, 1955) depicted in Fig. 1A, a configuration of four circular "pacman" elements generates the percept of a diamond-shaped object with sharp boundaries, which seems to occlude the adjacent circular elements. Such integration of parts into a coherent figure is commonly assumed to reflect the interpolation of the bounding contours and a filling-in process that renders the surface of the enclosed area of the illusory figure (Grossberg and Mingolla, 1985).

Neuronal activations in response to Kanizsa-type illusory figures (Fig. 1A, Kanizsa) are typically examined in relation to comparable control configurations, which consist of the same pacman inducers rotated such that no illusory figure is perceived (Fig. 1A, Baseline). This contrast may reveal potential mechanisms of object completion (e.g., Bakar et al., 2008; Mendola et al., 1999; Hirsch et al., 1995). For instance, responses specific to the emergence of an illusory figure were found to be located in areas V1 and V2 (von der Heydt et al., 1984; Peterhans and von der Heydt, 1989; Ffytche and Zeki, 1996; Seghier et al., 2000; Lee and Nguyen, 2001; Ritzl et al., 2003; Maertens and Pollmann, 2005; Kok and de Lange, 2014), but also in higher-order visual cortices such as the lateral occipital complex (LOC; Mendola et al., 1999; Stanley and Rubin, 2003), and sometimes also the fusiform gyrus (FG; Larsson et al., 1999; Bakar et al., 2008) – thus revealing involvement of both early and mid-level visual processing areas in illusory figure completion. Moreover, several studies have reported lateralization effects, with illusory figures tending to activate the right hemisphere more than the left (Hirsch et al.,
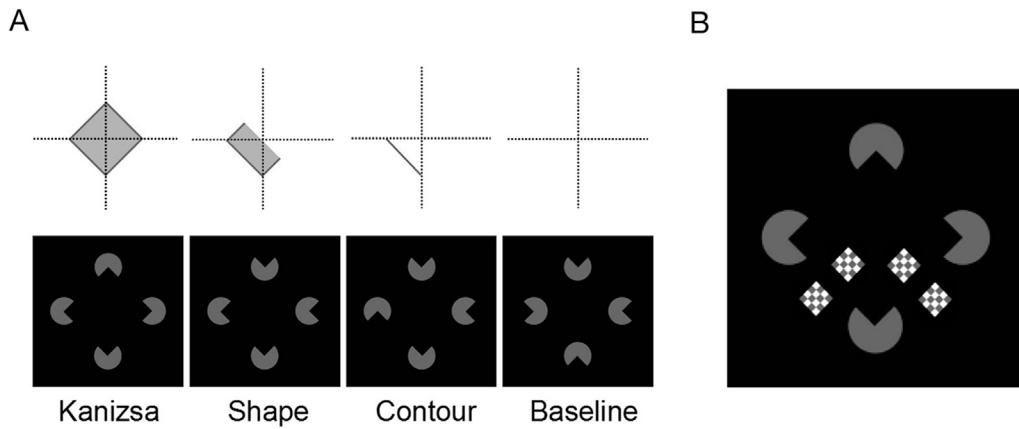
A

B

Fig. 1. (A) Examples of the stimuli used in the main experiment. Variants of all possible configurations (Kanizsa, Shape, Contour, Baseline) are depicted in the bottom panels. The top panels illustrate the corresponding emergent grouping, depicting the respective surface (gray) and contour (black) completions (with the strength of the illusory-figure representation increasing from right to left). See the text for further details. (B) Illustration of all possible locations of the checkerboards presented during the localizer session. Note that the reversing checkerboards appeared only at one of the four locations corresponding to the inside and outside locations in the bottom left or right quadrants of the presented configurations. The Kanizsa figure was not presented during the localizer scans; it is provided here only to illustrate the inside/outside locations relative to the configurations presented in the main experiment.

1995; Larsson et al., 1999; Halgren et al., 2003; see also Fink et al., 1996). Lateralized processing of whole objects is also supported by neuropsychological studies, which showed that patients with right-hemisphere posterior lesions are impaired at perceiving illusory figures, whereas patients with left-hemisphere lesions exhibit no difference relative to controls (Wasserstein et al., 1987; Grabowska et al., 2001).

However, these illusion-specific activations are likely to provide only a crude picture, since a variety of processes, including contour interpolation and surface filling-in, are thought to be involved (Grossberg and Mingolla, 1985; Pessoa et al., 1998) and various brain regions in the visual hierarchy are likely to contribute differentially to these component processes of completion (Grossberg and Mingolla, 1985; Grossberg, 2000; Kogo et al., 2010). For instance, early visual areas with their relatively small receptive fields have been suggested to predominantly encode edges and to be involved in processes of contour interpolation (Lamme, 1995; Zhaoping, 2003), while LOC, with its comparatively large receptive fields, plays a crucial role in figure-ground segregation and, thus, in the construction of bounded surfaces (Stanley and Rubin, 2003; Chen et al., 2018b). A potential approach to track the processes underlying the construction of a grouped object representation within a single experiment is to provide observers with "partial" groupings that target intermediate steps in the generation of complete-object representations. This approach was realized in the current study by an incremental manipulation of the grouping strength within a given stimulus configuration. More precisely: grouping of the pacman inducer elements was systematically varied such that these exhibited various "non-accidental" properties of an illusory figure, in particular, their surface portions and/or corresponding contour segments (Fig. 1A, Shape and Contour; see also Chen et al., 2018a).

As depicted in Fig. 1A, the Kanizsa configuration induces a complete illusory diamond (Kanizsa), whereas the "Shape" configuration provides only partial surface and contour information. The "Contour" configuration, by contrast, induces only a partial illusory contour without rendering concurrent surface information. Finally, the "Baseline" arrangement presents no grouped object, that is, no illusory figure, while consisting of similar inducer elements and a symmetric arrangement. Using this set of configurations, a recent study (Chen et al., 2018a) employed a spatial localization task in which observers had to judge whether a briefly presented dot-probe was located either inside or outside the illusory boundary of the configuration. Comparisons of these various configuration types revealed that perceptual (dot localization) sensitivity was highest for Kanizsa figures, intermediate for Shape and

Contour configurations, and lowest for Baseline configurations. These results show that grouping strength varies incrementally for these configurations, with more surface and contour information leading to stronger object representations that enhance dot (inside vs. outside) localization. Accordingly, employing these four types of configurations allows characterizing discrete stages in the construction of coherent object representations (see also Conci et al., 2006, 2007a; 2007b, 2009; 2018).

Using functional magnetic resonance imaging (fMRI), we examined whether neural activity is modulated by the completion of an object involving such a stepwise construction process. We used spatial localizers to locate brain regions (volumes of interest, VOIs) that respond to particular locations in the visual field representing illusory figure portions and acquired the blood-oxygen-level-dependent (BOLD) signals triggered by these various configurations in the localized brain regions. The approach, thus, was to trace the stepwise completion of an illusory figure by identifying BOLD signal changes that vary with grouping strength in these particular cortical regions, to determine their role in generating a complete-object representation in illusory figures. As a comparison, we also located brain regions that represented positions outside the illusory figure, where no completion occurs. We expected the neural activity of brain areas implicated in object completion to be incrementally modulated by increasing strength of the configuration, whereas no such modulation was expected in voxels coding the region outside the illusory figure.

Importantly, we also examined whether the potential effects of object completion occur automatically or under attentional control. In addition to the spatial localization task already described (requiring observers to localize a dot-probe as inside vs. outside the presented configuration; see above and Chen et al., 2018a), we also implemented a luminance discrimination task in which observers had to judge the brightness of the very same dot-probe (see Weidner and Fink, 2007; Plewan et al., 2012). Variation of the strength of the completed object was expected to modulate performance in the spatial localization task, facilitating target dot localization with respect to the critical (illusory) configuration boundary. In contrast, luminance discrimination of the same target dot can be performed irrespectively of any spatial completion operations, so that performance should be uninfluenced by variations of grouping strength. Accordingly, employing these two tasks allowed us to examine whether any activation patterns that reflect object completion mechanisms would manifest independently of the attentional demands of the two tasks.

2. Materials and methods

2.1. Participants

Twenty-three healthy right-handed participants (11 women) with normal or corrected-to-normal visual acuity participated in the fMRI experiment. Participants' ages ranged from 20 to 45 (median = 27) years. All participants were remunerated for their participation and gave informed written consent before the experiment. The experimental procedure was approved by the Ethics Committee of the Department of Psychology, Ludwig-Maximilians-Universität München. The sample size was determined based on the effect sizes derived from previous, comparable fMRI studies (e.g., Maertens et al., 2008; Kok and de Lange, 2014; Mendola et al., 1999), which yielded a large effect size (with f(U) values ranging between 0.8 and 1.4). On this basis, our sample size would be sufficient to detect a difference between Kanizsa and Baseline configurations (in a repeated-measures analysis of variance) with 85% power and an alpha level of 0.05. Power estimates were computed using G*Power (Erdfelder et al., 1996).

2.2. Stimuli

Stimuli were generated by an IBM-PC compatible computer using Matlab routines and Psychophysics Toolbox extensions (Brainard, 1997; Pelli, 1997), and were presented in light gray (RGB: 103, 103, 103) against a black (RGB: 0, 0, 0) background at the center of a 30-inch shielded LCD monitor mounted outside the MRI scanner on the wall behind the participant's head. The screen was located at a distance of 245 cm from the participant and was seen via a mirror on top of the head coil.

There were four types of experimental stimuli (see Fig. 1A): (1) a Kanizsa diamond configuration (Kanizsa) that presented a complete illusory figure; (2) a shape configuration that depicted partial contour and surface completions (Shape); (3) a configuration that only induced an illusory contour without an associated surface (Contour); and (4) a control configuration that consisted of four 'pacman' inducers with their indents facing away from the stimulus center, thus, rendering a symmetric arrangement without any emerging shape (Baseline). Each pacman inducer subtended a visual angle of 1.5°. The radius of the illusory diamond shape was 2.7° of visual angle. The support ratio (Banton and Levi, 1992), that is, the ratio between the luminance-defined portion and the completed illusory contour, was 0.4, thus giving rise to a clearly visible illusory figure.

The target stimulus was a small dot-probe (9 arc-min in diameter), which was presented in light (RGB: 220, 220, 220) or dark (RGB: 78, 78, 78) gray randomly near the bottom left or right illusory edge of a given pacman configuration. The target appeared randomly at one of two equidistant locations along the midline perpendicular to the bottom left or right border of the illusory figure (−14 or +14 arc-min from the center point of the border). These stimulus location parameters were shown in our previous, behavioral study (Chen et al., 2018a) to reveal the most reliable and most substantial difference in performance across the four configuration conditions.

2.3. Procedure and design

Each trial started with the presentation of a central fixation cross for 200 ms, followed by a 900-ms display presenting one of the four configuration conditions (Kanizsa, Shape, Contour, or Baseline). Next, a (target) dot-probe was added to the display and presented for another 100 ms (see Fig. 2). Each trial block in the experiment was dedicated to present one of the four configurations (Kanizsa, Shape, Contour, and Baseline), with the target appearing consistently in either the lower left or lower right quadrant of the stimulus display, with block order randomized across participants. We probed the lower quadrants of the display because the lower hemifield has been shown to produce a stronger percept of an illusory figure than the upper hemifield (Rubin et al., 1996). To examine whether object integration occurs automatically, we additionally manipulated the attentional demands using two tasks: a spatial localization and a luminance discrimination task. In the *spatial localization task*, participants had to indicate whether the target dot was located inside or outside of the perceived illusory region enclosed by the inducers. Subjects responded by pressing the left and right button with their left (inside) or right (outside) index finger, respectively. Participants were provided with instructions, which included illustrations of the correct boundary that determines the inner region of the displayed configuration (see Chen et al., 2018a). Note that the boundary of a given configuration was always located at the very same position on the screen for all types of configuration. In the *luminance discrimination task*, participants had to indicate whether the target dot was light or dark gray, by responding with the left or right index finger, respectively (as in the spatial localization task). The physical stimuli were the same in both the spatial localization and the luminance discrimination task. Note that variations in the strength of the completed object will potentially facilitate localizing the target dot near the illusory boundary, thus modulating performance in the spatial localization task. By contrast, the luminance discrimination could be effectively performed independently of any spatial completion operations, so that variations of
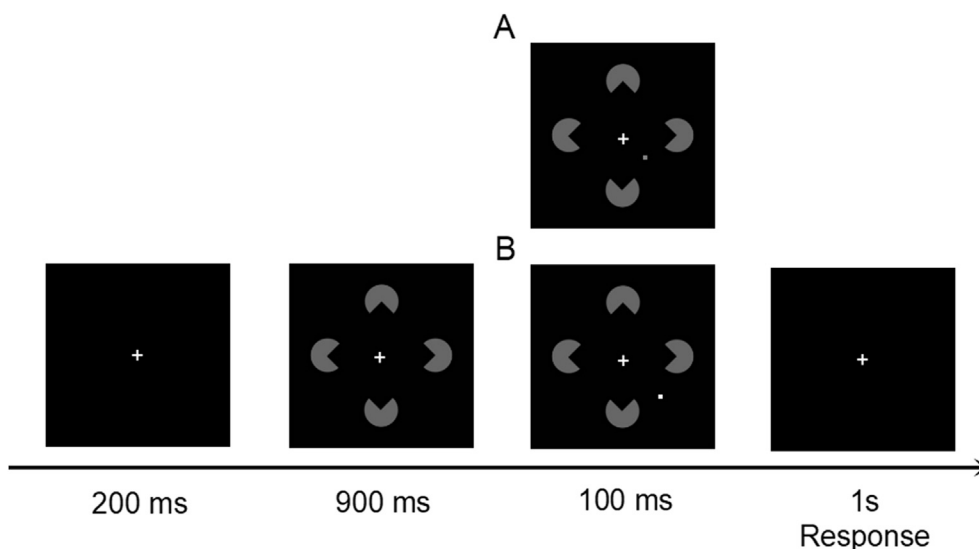

Fig. 2. Example trial sequence in the main experiment. Following a fixation cross (200 ms), a configuration (either Kanizsa, Shape, Contour, or Baseline) was briefly presented (900 ms), after which the target (i.e., the dot-probe) was added and presented for another 100 ms. In the example, the target is presented near the bottom-right boundary of the enclosed region. Observers were instructed to i) report whether the target was light or dark gray in the luminance discrimination task (here, the correct response would be 'dark' in display A and 'light' in display B), or ii) indicate whether the target appeared inside or outside the enclosed illusory region in the spatial localization task (in the example, the correct response would be 'inside' in display A and 'outside' in display B).

grouping strength should not influence performance (while an automatic completion process should nevertheless modulate the neuronal responses).

For the main experiment, a single run was recorded. Stimuli were presented in 80 consecutive blocks, each consisting of eight trials (2.2 s duration per trial). A sequence of 8 blocks always involved the same task. Before each task 'session' (of 8 blocks), a semantic cue was presented for 5 s, informing participants which task (luminance discrimination or spatial localization) they were to perform. A blank screen with a fixation cross was presented for 5 s before and after each task session. Task sessions were presented in a randomized order, separated by intervals in which either the fixation cross or the task instruction was present on the screen. Observers were instructed to fixate a central cross throughout the entire experiment. The overall experiment took about 32 min to complete. Before the experiment, participants were acquainted with the tasks in a practice session of 128 trials, which was performed outside the scanner.

We used a spatial localization procedure, administered before the main experiment, to identify brain regions and the neural populations responding to specific positions in the visual field. In this procedure, participants viewed alternating 16-s blocks of a reversing checkerboard ($1.1° × 1.1°$, 10 Hz, gray and white checks, RGB: 103,103,103 and RGB: 255, 255, 255, respectively). The checkerboard stimuli were presented at positions corresponding to the inside or outside locations of the dot-probe stimulus in the main experiment. This procedure permitted us to functionally identify VOIs corresponding to the visual cortical representations of the inside and outside probed regions in the main experiment (see Fig. 1B). The localizer checkerboard stimuli were presented in the bottom left or right visual field quadrants on a black background (RGB: 0, 0, 0), at locations either inside or outside the illusory figure in the experiment proper (see Fig. 1B; note that no illusory figures were presented during the localizer scans – the Kanizsa figure is just added in Fig. 1B for purposes of illustration). Each localizer was presented four times at each of the four locations, resulting in a total of 16 blocks. Blocks were separated by intervals of 5 s, during which a fixation cross was presented. A blank screen with a fixation cross was presented for 10 s at the start and the end of the localizer session. The duration of the localizer session was around 6 min. During the entire session, participants were asked to fixate the cross at the center of the screen.

2.4. fMRI measurement

2.4.1. Data acquisition

Functional imaging data were acquired using a 3-T TRIO MRI system (Siemens, Erlangen, Germany) and T2* weighted EPI sequences (repetition time = 2.2 s, echo time = 30 ms). For the main experiment, a total of 874 vol and for the position localizer a total of 245 vol of 36 axial slices were acquired using an interleaved slice mode (thickness = 3 mm, distance factor = 10%, field of view = 200 mm, 64 × 64 matrix, in-plane voxel size = $3.1 × 3.1$ mm^2).

2.4.2. Data preprocessing

The fMRI data were analyzed using the statistical parametric mapping software SPM12 (Wellcome Department of Imaging Neuroscience, London; http://fil.ion.ucl.ac.uk/spm/software/spm12). The first five images were excluded from analysis, as these were acquired before the MR signal had reached its steady state. Images were first spatially realigned to correct for inter-scan movement and spatially normalized to match the MNI single-subject template using the unified segmentation function in SPM12. The data were then smoothed using a Gaussian kernel of 8 mm FWHM.

2.5. Data analysis

Three participants exhibited relatively high error rates (above 30%

errors overall, exceeding three standard deviations above mean performance) and were thus excluded from further analyses. Accordingly, the data analyses reported below are based on a sample of 20 participants (10 male, mean age: 27.5, SD = 6.4, years).

2.5.1. Behavioral data analysis

For the behavioral analysis, a repeated-measures analysis of variance (ANOVA) was performed on the accuracy and reaction time (RT) data with the within-subject factors Task (luminance, localization) and Configuration (Kanizsa, Shape, Contour, Baseline). Note that targets presented in the left and right hemifields were collapsed for this analysis. Trials with RTs faster than 200 ms were considered as anticipations and excluded from further analysis; also, error trials were removed before the RT analysis.

2.5.2. Functional analysis: main experiment

Sixteen onset regressors were defined, thus, reflecting the 16 different experimental conditions (2 tasks × 4 configurations × 2 sides). The hemodynamic response was modeled using a canonical hemodynamic response function and its time derivative. Error trials (incorrect/missing responses and trials with RTs faster than 200 ms) were modeled in a single additional regressor. Linear and quadratic effects of the six head movement parameters were included as additional regressors in the design matrix.

To specify the first-level contrasts, each experimental regressor was compared with the implicit baseline. The resulting contrast images were subjected to a second-level flexible factorial design with "conditions" as within-subject factor and participants as a random factor, implementing a random-effects analysis. We focused on the analysis of effects of illusion (i.e., the comparison between Kanizsa and Baseline configurations) by using planned t-contrasts, thresholded at $p < .05$ familywise error, whole-brain corrected at the cluster-level (with cluster-defining voxel-level cutoff of $p < .001$).

2.5.3. Functional analysis: position localizers

VOIs in visual cortical areas were identified using localizer stimuli (checkerboards) at four positions corresponding to the inner and outer regions in bottom-left and -right visual field quadrants (Fig. 1B). Four regressors marking the onsets of the visual stimulation conditions (duration = 16 s) at the four different localizer positions were defined. The hemodynamic response for each condition was modeled using a hemodynamic response function and its time derivative. Six head movement parameters were included in the design matrix as additional regressors. A first-level analysis was conducted comparing each onset regressor with the remaining three onset regressors. The resulting contrast images were subjected to one-sample t-tests thresholded at $p < .05$ familywise error, whole-brain corrected at the cluster-level (with cluster-defining voxel-level cut-off of $p < .001$). VOIs were defined as spheres (radius = 3 mm) centered at the group maxima within the significant clusters of the second-level contrast image. The separate VOI areas were labeled according to the probabilistic atlas provided by Wang et al. (2015)in MNI space. Thus, despite the different sizes of activated clusters observed in the whole-brain analyses, the number of voxels used for the VOI analysis was identical. Moreover, the estimated BOLD amplitudes in the main experiment (i.e., when presenting a specific stimulus configuration) were based on identical numbers of voxels. Beta values were then analyzed employing a two-way repeated-measures ANOVA with the factors Task (luminance, localization) and Configuration (Kanizsa, Shape, Contour, Baseline) at different VOIs.

3. Data availability statement

Participants' data used in this study are not publicly available, but will be made available, by the corresponding author, upon reasonable request (for research purposes only).

4. Results

4.1. Behavioral data

The mean accuracies across participants are depicted in Fig. 3. Participants performed significantly better in the luminance discrimination task ($M = 92\%$) as compared to the spatial localization task ($M = 81\%$), F (1, 19) = 63.47, $p < .0001$, $\eta_p^2 = 0.77$. There was also a main effect of Configuration, $F(3, 57) = 22.43$, $p < .0001$, $\eta_p^2 = 0.54$, indicating that performance varied for the different stimulus configurations. The interaction of Task and Configuration was also significant, $F(3, 57) = 22.12$, $p < .0001$, $\eta_p^2 = 0.54$. While performance showed no difference among configurations in the luminance discrimination task (92%, 93%, 92%, and 92% for Kanizsa, Shape, Contour, and Baseline, respectively; $ps > .14$), it was significantly modulated by Configuration in the spatial localization task: accuracy was highest for Kanizsa (86%) and Shape (85%) configurations, intermediate for the Contour configuration (80%), and lowest for the Baseline configurations (74%) (all $ps < .001$, except for the comparison between Kanizsa and Shape configurations, $p = .61$). This pattern of results shows that a behavioral difference among the various configurations was evident only in the spatial localization task, in which the spatial configuration was task-relevant, that is: performance depended on both task and configuration variations.

In a subsequent step, we arcsine-transformed the accuracy data to correct for potential "end-of-scale" effects, that is, to exclude the possibility that the absence of a significant configuration effect in the luminance discrimination task was due to a ceiling effect. The result pattern for the arcsine-transformed accuracies remained the same as described above, revealing significant main effects of Task, $F(1, 19) = 71.33$, $p < .0001$, $\eta_p^2 = 0.79$, and Configuration, $F(3, 57) = 12.80$, $p < .0001$, $\eta_p^2 = 0.40$, and an interaction between Task and Configuration, $F(3, 57) = 12.71$, $p < .0001$, $\eta_p^2 = 0.40$. There was again no difference between the configurations in the discrimination task ($ps > .24$), whereas there were significant differences in the localization task (all $ps < .001$, except for the difference between Kanizsa and Shape, $p = .58$). Thus, these differential performance patterns cannot be attributed to a ceiling effect in the luminance discrimination task.

Finally, for the analysis of the mean RTs, a comparable ANOVA as above revealed no significant effects (*mean* RTs: 535 ms, $SD = 55$), indicating that there was no trade-off between the accuracy and RT measures.

4.2. Functional imaging data

Neural activations associated with the emergence of an illusory figure were examined by contrasting trials that presented Kanizsa figures with trials that presented Baseline configurations. Activations that were positively associated with the illusory Kanizsa figure were detected in
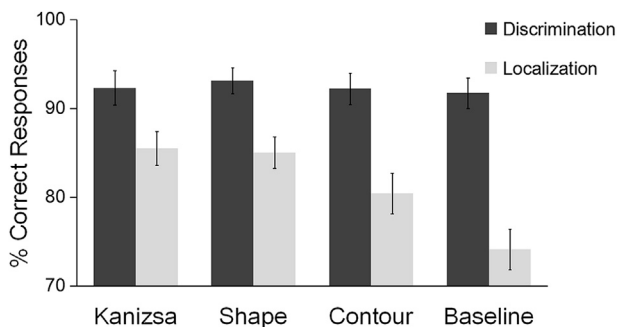

Fig. 3. Mean percentage of correct responses in the luminance discrimination and spatial localization tasks, for the different stimulus configurations (Kanizsa, Shape, Contour, and Baseline). Error bars denote 95% (within-subject) confidence intervals.

LOC, reaching from the inferior occipital gyrus (IOG) to the middle occipital gyrus (MOG), and into the fusiform gyrus (FG; see Fig. 4A). In order to focus on the particular locations in the visual field that represented illusory figure portions, the regions activated by the functional localizers were labeled according to the probabilistic atlas of Wang et al. (2015, see Fig. 4B). The left and right inner checkerboards activated areas V1 (including V1v and V1d), V2 (including V2v and V2d), V3 (including V3v and V3d), V3a, hV4, hMT, LO1, and LO2 (extending to FG). The left and right outer checkerboards activated V1, V2, V3a, and V3d. For further analysis, we defined different functional VOIs based on the clusters activated by the functional localizers, specifically: VOI spheres of radius 3 mm centered at the peak activation location of the significant clusters corresponding to the inner and outer regions in human V1 and LOC (LO1 and LO2), according to the Wang et al. (2015) probability maps. We did focus on these VOIs because, in prior studies, illusion-specific activations within the regions related to our inner localizers had mainly been reported in areas V1 and LOC (e.g., Maertens and Pollmann, 2005; Kok and de Lange, 2014; Mendola et al., 1999; Stanley and Rubin, 2003). In more detail, the VOIs coding the regions inside the stimulus configurations, as induced by the left and right inner checkerboards, respectively (purple, Fig. 4C), were located mainly in the right (group maxima: 40, −76, 0) and left LOC (group maxima: −36, −86, 6; purple, Fig. 4B), and in V1 (group maxima in the right hemisphere: 22, −88, 6; group maxima in the left hemisphere: −18, −94, 2). Specifically, the left inner VOI in the LOC region was located in both areas LO1 and LO2, whereas the right inner VOI in the LOC region was located in LO2 only. VOIs coding regions outside the Kanizsa figure, as induced by the left and right outer checkerboards (blue, Fig. 4C), were identified only in V1 (group maxima in the right hemisphere: 18, −92, 12; group maxima in the left hemisphere: −12, −94, 10; blue, Fig. 4B), while there was no significant activation in LOC.

First, the beta values representing BOLD-amplitudes estimated in the main experiment were extracted from the voxels within the different VOIs. Beta values were combined for left and right V1 of the inner VOI, for left and right LOC of the inner VOI, and for left and right V1 of the outer VOI. An initial analysis compared the average BOLD signals of these three VOIs that exhibited significant peak activations (i.e., inner V1, inner LOC, and outer V1), which revealed no significant differences among the VOIs, $F(2, 38) = 1.61$, $p = .21$, $\eta_p^2 = 0.08$. This indicates that the three VOIs were overall comparable in terms of their average activations.

In a subsequent step, the beta values were compared across the various experimental conditions. First, the average BOLD signal of the left and right V1 of the inner VOI revealed no significant effects of Stimulus Configuration or Task ($ps > .11$; Fig. 4D, V1). However, for the average signals of LOC representing the inner VOI, there was a main effect of Configuration, $F(3, 57) = 5.77$, $p = .002$, $\eta_p^2 = 0.23$. As depicted in Fig. 4D (LOC), the signal strength was highest for the Kanizsa configuration (0.36), followed by the Shape (0.24) and Contour (0.18) configurations, and lowest for the Baseline (−0.003) configuration ($ps < .05$, though the difference between Shape and Contour was not significant: $p = .44$). The effect of Task was not significant (spatial localization vs. luminance discrimination: 0.26 vs. 0.13, respectively), $F(1, 19) = 3.09$, $p = .095$, $\eta_p^2 = 0.14$, and there was also no interaction ($p = .56$). This finding shows that stimulus configuration modulated the activations in LOC independently of the task. Finally, for the average BOLD signals of left and right V1 of the outer VOI, there was again no significant difference among the various stimulus configurations and across tasks ($ps > .21$, see Fig. 4E), indicating that the representation of the outside dot locations was not affected by changes in the strength of object completions.

Further, to compare the effect of completion as observed in the behavioral data with the (inner) LOC signal modulation, the accuracies in the localization task and BOLD signals in the Kanizsa configurations were subtracted from the respective values in the Baseline configuration, with the resulting difference revealing the "net" effect of object completion.
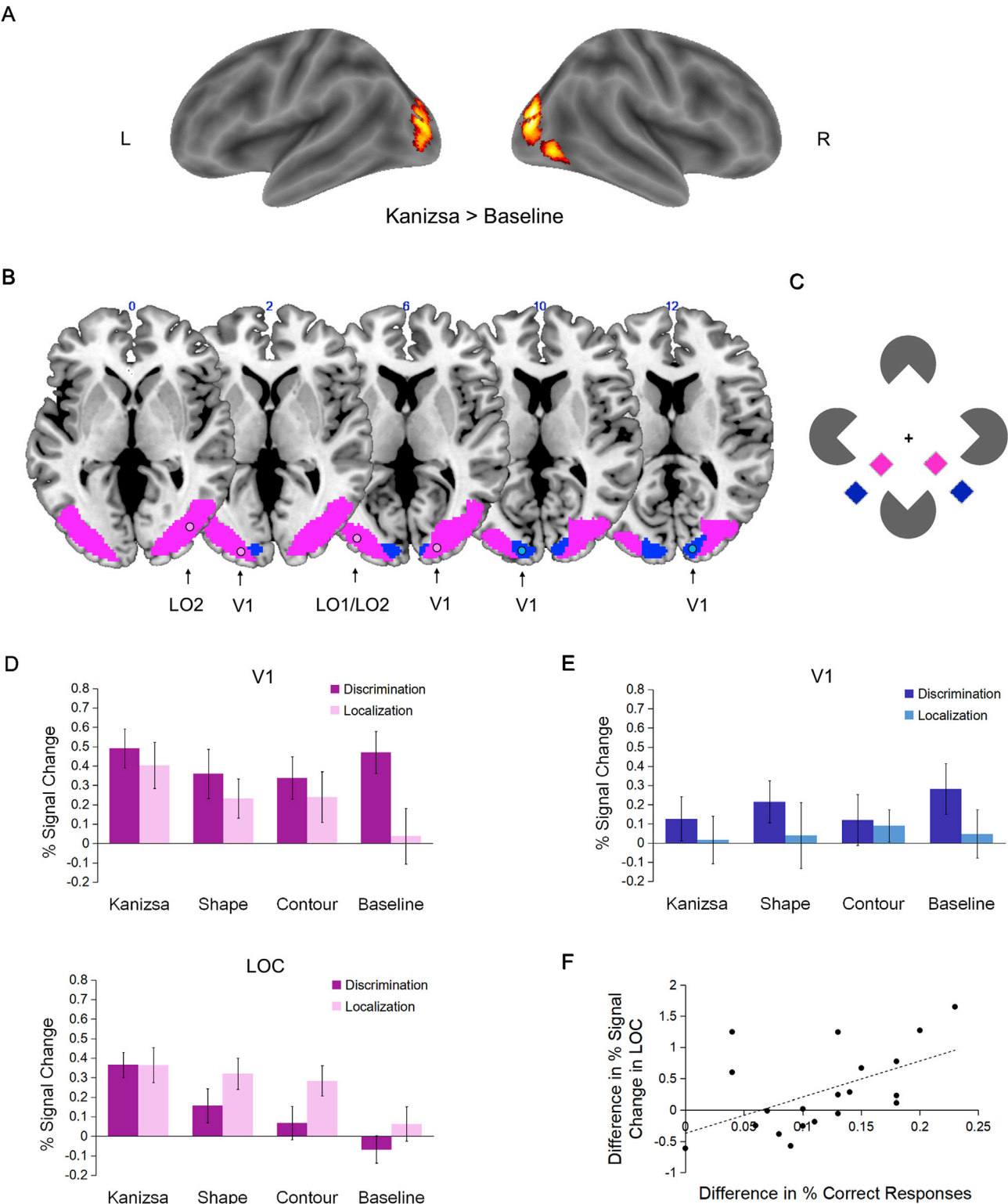
Fig. 4. A. Surface rendering of the fMRI results obtained in the whole-brain analysis, depicting the activations related to the illusory Kanizsa figure. Views are shown from the left and right viewpoints. The Kanizsa vs. Baseline contrast was thresholded at $p < .05$ familywise error, whole-brain corrected at the cluster-level (with cluster-defining voxel-level cutoff of $p < .001$). **B.** Increased visual activations induced by the four different position localizers (of the left inner, right inner, left outer and right outer quadrant) are projected onto a two-dimensional slice-based, medial view of the brain. VOIs with spheres of 3-mm radius (corresponding to the black circles in the figure) were centered at the peak location of the significant clusters corresponding to the inner (purple) and outer regions (blue) as induced by the different position localizers and were labeled according to the probabilistic atlas provided by Wang et al. (2015), including probability maps of human V1 and LOC (LO1 and LO2). Specifically, the left inner VOI in the LOC region (purple) was located in both areas LO1 and LO2 (group maxima: −36, −86, 6), whereas the right inner VOI in the LOC region was located in LO2 only (group maxima: 40, −76, 0). The left inner VOI coding the regions inside the Kanizsa figure was also located in the V1 (group maxima in the right hemisphere: 22, −88, 6; group maxima in the left hemisphere: −18, −94, 2; purple). VOIs coding regions outside the Kanizsa figure were identified only in V1 (group maxima in the right hemisphere: 18, −92, 12; group maxima in the left hemisphere: −12, −94, 10; blue). **C.** Position localizers denoting inner (purple squares) and outer (blue squares) positions in the bottom left and right visual field quadrants of the stimulus display. **D.** Mean % of signal change in regions of bilateral V1 and LOC with a receptive field in the inner bilateral VOIs (the purple circles in panel B). **E.** Mean % of signal change in regions of bilateral V1 with a receptive field in the outer bilateral VOIs (blue circles in panel B). **F.** Correlation between the difference between Kanizsa and Baseline configurations (providing a measure of completion) in LOC signals and the corresponding accuracy difference in the localization task. Error bars denote within-subject SEMs.

Subsequent analysis revealed a significant correlation between the difference in accuracy and the corresponding difference in LOC activations, $r = 0.52$, $p = .019$ (two-tailed; see Fig. 4F). The statistical significance of the correlation coefficient was determined by comparing the observed correlations with results derived from 5000 permutations of the two variables. This procedure ensures that the significant correlation is not attributable to any outliers in the data. The correlation thus indicates that the behavioral completion effect was directly related to the pattern of activation in LOC.

An additional analysis was performed to test further whether the grouping of the illusory figure modulated the BOLD amplitude independently of the target dot location. For instance, for the Kanizsa diamond, the integration of the pacmen inducers should lead to an activation pattern that spreads to the whole figure (including the non-attended display hemifield). We, therefore, compared the activations within the inner LOC VOIs between the Kanizsa and Baseline configurations in response to both ipsilateral and contralateral target locations. A repeated-measures ANOVA with the factors Configuration, Task, and Side was performed, which yielded a significant main effect of Configuration in (inner) LOC, $F (1, 19) = 17.88, p < .0001, \eta_p^2 = 0.49$, reflecting higher activations for Kanizsa figure ($M = 0.25$) compared to Baseline configurations ($M = -0.08$) regardless of the target side or task (see Fig. 5). By contrast, there were no significant effects of Configuration or relevant interactions in V1 for the inner or outer VOIs ($ps > .17$). Taken together, this pattern of results shows that LOC was implicated in coding the representation of the illusory figure in both halves of the display, indicative of spreading of the grouped region within the boundaries of the entire configuration.

Next, to further quantify the activation patterns induced by the position localizers inside the illusory configuration, the inner VOIs in the left and right hemispheres were assessed in separate analyses. The results of this analysis are depicted in Fig. 6A/B, with the bar graphs displaying the mean BOLD amplitudes within each of the predefined inner VOIs (Fig. 6C), plotted separately for the different target quadrants in the various experimental conditions.
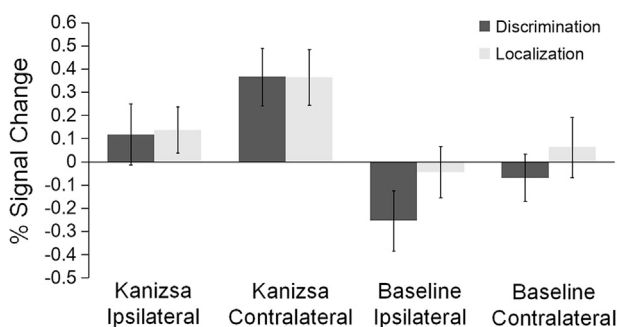
The analysis of the left inner VOI in V1 (Fig. 6A upper panel) revealed no significant effects, $ps > .18$. However, for the left inner VOI in area LOC (Fig. 6A bottom panel), main effects of Task, $F (1, 19) = 4.91, p = .039, \eta_p^2 = 0.21$, and Configuration were found, $F (3, 57) = 3.84, p = .014, \eta_p^2 = 0.17$, reflecting an overall reduced signal strength for the luminance discrimination task ($M = 0.12$) compared to the spatial localization task ($M = 0.30$). In addition, the BOLD signals were reduced for the Baseline ($M = -0.08$) as compared to Kanizsa ($M = 0.29$; $p = .009$), Shape ($M = 0.28$; $p = .024$) and Contour ($M = 0.35$; $p = .002$) configurations, without any differences among Kanizsa, Shape, and Contour stimuli ($ps > .31$). Thus, left LOC was found to be sensitive to both task demands and (any) spatial regularity inherent in the stimuli.

By contrast, for the right inner VOI in V1 (Fig. 6B upper panel), there was only a main effect of Configuration, $F (3, 57) = 4.39, p = .008, \eta_p^2 = 0.19$, with an enhanced signal for the Kanizsa configuration ($M = 0.73$) as compared to Shape ($M = 0.29$), Contour ($M = 0.26$), and Baseline ($M = 0.15$) configurations ($ps < .006$), and no significant differences between the other three configurations ($ps > .21$), thus indicating that this region was especially sensitive to the complete-object configuration independently of the task. Next, the results for the right inner VOI in area LOC (Fig. 6B bottom panel) again revealed a main effect of Configuration only, $F (3, 57) = 5.12, p = .003, \eta_p^2 = 0.21$, characterized by an increased signal strength for the Kanizsa configuration ($M = 0.44$) as compared to Shape ($M = 0.21$), Contour ($M = 0.005$), and Baseline ($M = 0.08$) configurations ($ps < .035$), alongside a higher signal for Shape as compared to Contour configurations ($p = .026$) and no difference between Contour and Baseline configurations ($p = .75$). Thus, right LOC was activated independently of the task at hand and its activation scaled with the amount of surface rendered in a given configuration.

5. Discussion

Illusory figures attest to the power of perceptual grouping in human vision. Using fMRI combined with spatial functional localizers, the current study investigated discrete steps of processing by which parts are integrated into a coherent whole in the human cerebral cortex. To tackle this issue, we systematically manipulated grouping in the presented stimulus configurations, such that these exhibited a graded amount of contour and surface completions in the left and right hemifields, allowing us to track changes in the neural activity induced by the configurations as a function of (incremental) grouping strength.

The behavioral results revealed detection accuracies to be modulated by both the amount of surface and contour completion present within a given configuration. Configurations that rendered a complete object supported higher spatial localization performance than partial surface and contour configurations, which in turn supported a higher level of performance than the ungrouped baseline. This graded change in performance as a function of the grouping strength inherent in these configurations replicates previous findings (Chen et al., 2018a). Of note, however, this influence of the configuration was evident only in the spatial localization task, when the configural layout was directly
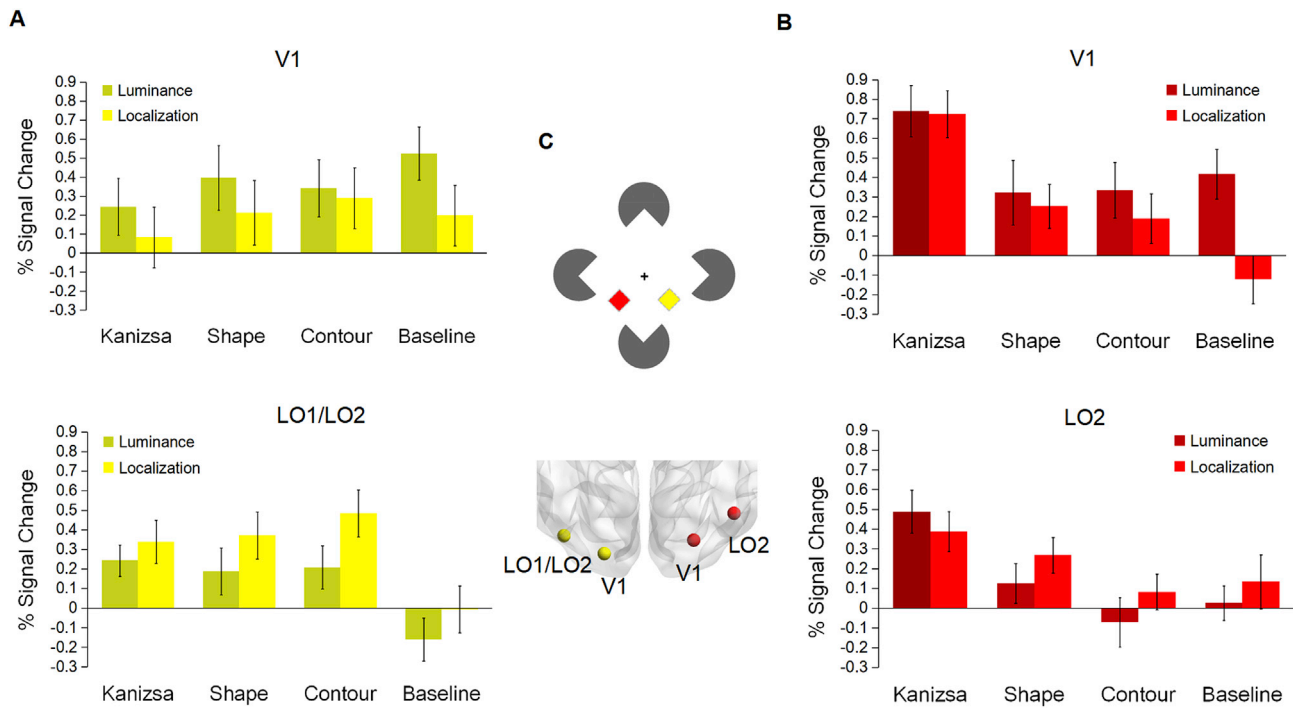
Fig. 5. Mean % signal change for Kanizsa and Baseline configurations in bilateral LOC within the inner VOIs ipsi- and, respectively, contralateral to the target dot. Error bars denote within-subject SEMs.

Fig. 6. Neural activity modulations by experimental conditions in inner VOI locations, separately for the left and the right hemisphere (as induced by targets presented in the right and the left visual field quadrant, respectively). **A.** BOLD response in regions of V1 and LOC (LO1/LO2) in the left hemisphere (the yellow area in panel **C**). **B.** BOLD response in regions of V1 and LO2 in the right hemisphere (the red area in panel **C**). **C.** Inner VOIs (lower panel) induced by the position localizers inside the configuration (upper panel). Error bars denote within-subject SEMs.

task-relevant. By contrast, no comparable modulation was evident in the luminance discrimination task, in which the spatial organization of the display was irrelevant for solving the task. In contrast to the luminance discrimination task, in which the judgment was exclusively based on the probe itself (its lightness), the spatial localization task required an estimate of the location of the dot relative to the surrounding pacmen – and for this, object completions render a more precise estimate of the target's spatial position. In other words, grouping increases the precision of spatial judgments by integrating parts into a coherent shape.

Brain regions coding the locations inside the (partial) illusory figure predominantly involved LOC. Average BOLD signals of left and right LOC coding the illusory figure (in response to both left and right hemifields) were modulated incrementally by an increase in grouping strength, that is, the stepwise emergence of a whole-object representation (e.g., as illustrated in Fig. 1A). Moreover, the bilateral LOC in the inner VOIs was involved in coding the whole illusory figure, irrespective of the location of the target dot, indicative of a spreading of the illusory surface in LOC. The processing of the completed object in LOC was further evidenced by a positive correlation between the effects of grouping in the BOLD signals (in LOC) and behavioral precision. While there was a clear-cut effect of grouping in LOC, no comparable effect was evident in the corresponding inner and outer VOIs in V1. However, larger regions were found to be activated by the inner than by the outer localizer. The latter is consistent with previous estimates of response-field size in human visual areas, according to which the field sizes of voxel responses increase with eccentricity (Smith et al., 2001), with a greater rate of increase in higher-tier visual areas, such as LOC, than in early visual areas (Larsson and Heeger, 2006). In the outer VOI in bilateral V1, the activations were not modulated by the various configuration conditions – in contrast to the inner VOIs, where the neural activation pattern in LOC appeared to directly reflect object construction processes, though comparable activations were found in the VOIs representing regions inside and outside the illusory figure. Of note, Kok and de Lange (2014) also used a localizer procedure to compare responses to an illusory figure to a baseline configuration that did not give rise to such a figure. They found that

neural activity in regions that specifically responded to the pacman inducers was not significantly modulated by the presence versus the absence of an illusory figure. By contrast, regions corresponding to the location of the illusory figure exhibited an increase in activation. This pattern indicates that illusory-figure-specific activations are predominantly representing the completed object, rather than the inducing pacmen.

To gain a more detailed picture, we further compared left and right hemisphere activations in response to the (partial) illusory figures presented in the right and left hemifields, respectively. Our experimental stimuli exhibited an incremental change of their inherent grouping properties, in that they depicted emerging contours and surface regions. For instance, contour interpolations occurred for all configurations with object-specific regularities (Kanizsa, Shape, and Contour configurations), and a corresponding surface was rendered, in particular, in Kanizsa and Shape configurations. These regularities were reflected in different patterns of activation in left and right LOC, with overall stronger responses in right LOC to the global shape than to detailed contour information; by contrast, there was no significant difference between global shape and contour information in left LOC. An asymmetric hemispheric activation was also observed in V1, with enhanced responses in the right V1 specifically for the complete Kanizsa figure, whereas there was no difference among any of the configurations in the left V1. Our finding of a right-hemispheric dominance in global shape processing is in accordance with previous reports of a right-hemispheric lateralization in lower and mid-level visual areas in illusory-figure processing (Hirsch et al., 1995; Larsson et al., 1999; Halgren et al., 2003).

While right LOC was more involved in global shape processing, left LOC was found to be sensitive to all configurations that exhibited (at least) parts of an integrated object. It has been suggested that the left hemisphere, and the inferior occipital lobe, in particular, encode edges and textures, whereas the right hemisphere predominantly extracts surface and luminance properties (Iidaka et al., 2004; Peyrin et al., 2004). Comparable lateralization of global object information has also been reported for the right hemisphere, while the processing of local details is

more lateralized to the left hemisphere (Marshall and Halligan, 1995; Fink et al., 1996, 1997; Han et al., 2002). The current results agree with these observations in suggesting that both hemispheres make differential contributions to the generation of a completed object: while the right hemisphere processes a global object representation, the left hemisphere is implicated in the concurrent processing of regularities at a finer scale. Moreover, a segmentation of the human LOC into separable sub-regions revealed two visual field maps, LO1 and LO2, that may be distinguished (see Larsson and Heeger, 2006; Wang et al., 2015). It has been suggested that LO1 and LO2 integrate shape information from multiple visual sub-modalities in retinotopic coordinates, with segregation of function between the two areas: while LO1 primarily extracts boundary information, LO2 codes regions and represents shape (Larsson and Heeger, 2006). Based on the probabilistic atlas of Wang et al (2015), we found the left inner VOI in LOC to be located in both areas LO1 and LO2 and to be involved in the processing of both surface and boundary information, whereas the right inner VOI in LOC was confined to LO2 only and processed surface information. This result suggests that our data not only accord with the functional specialization across hemispheres (see above), but also mirror the previously suggested difference in the response properties between LO1 and LO2.

Interestingly, Kanizsa and Shape configurations, which present an identical image in one half of the display, nevertheless engendered a difference in the activation pattern in the right V1. This finding is consistent with Peterhans and von der Heydt (1989), who found neurons in the early visual cortex to respond more strongly to a complete illusory figure than to a configuration in which half of the figure was removed. Moreover, judging the curvature of an illusory contour is also known to lead to a severe performance deficit when the to-be-judged illusory contour passes the blind spot under monocular viewing conditions (Maertens and Pollmann, 2007). Given that an interruption of the retinotopic visual field representation at the blind spot is specific to V1 (Awater et al., 2005), such a reduction of illusory-contour processing would imply that illusory-contour integration by adjacent collinear neurons requires V1. However, since V1 comprises relatively small receptive fields, some long-range connections, conveying information from the inducers in the opposite hemifield, are likely to be additionally involved in integrating information from the illusory figure.

The stepwise emergence of a whole-object representation allows us to trace the construction of both contours and surfaces at the neural level. Our findings – especially the modulation of neural signaling by incremental changes in grouping strength, particularly in LOC – indicate that various "non-accidental" properties such as contours and surfaces are integrated within LOC. These findings are at variance with the view that independent (but complementary) systems are involved in the completion of contours and surfaces (Grossberg and Mingolla, 1985; see also Grossberg, 2000). For instance, early visual areas with their relatively small receptive fields encode edges or are involved in contour interpolation (Zhaoping, 2003; Lamme, 1995), while LOC, with its comparatively large receptive fields, plays a crucial role in figure-ground segregation and, thus, the construction of bounded surfaces (Stanley and Rubin, 2003; Chen et al., 2018b) and the generation of a coherent illusory figure (Kourtzi and Kanwisher, 2001; Mendola et al., 1999). Our results suggest that, while V1 is involved in Kanizsa-figure processing, various grouping properties within a visual scene are nevertheless integrated predominantly in LOC, with sub-regions in the left and right hemispheres specializing in component sub-processes that render completed objects.

A possible scheme for explaining the dominant role of LOC in object completion processes assumes that object fragments are first analyzed in the primary visual cortex before converging on cells in higher-order visual cortical regions such as LOC (Spillmann and Werner, 1996). LOC, in turn, constructs a global, complete-object shape (Vuilleumier et al., 2002; Cox et al., 2013; Kubilius et al., 2011), where the output of these computations is re-projected to early visual areas (such as V1). Accordingly, modulations in right V1 in response to complete illusory figures might

reflect feedback from higher-order visual regions with the purpose of processing the whole object's finer details. For instance, such recurrent processing might strengthen the segregation of the (illusory) figure from the background and sharpen the contour representation (see also Stanley and Rubin, 2003; Roelfsema, 2006).

Note that these object-specific modulations in LOC were seen with both tasks employed in the current study, even though they involved different 'attentional' requirements regarding the need to incorporate the grouped layout for performing the task: localization of the target dot with respect to the illusory boundary would be supported by shape completion, whereas performing the luminance discrimination task would not, per se, require engaging in figure completion. In line with this, behavioral performance was modulated by the grouping strength only in the spatial localization task, but not in the luminance discrimination task. By contrast, the neural signals in LOC exhibited the very same modulation irrespective of the task. In other words, neural activity was modulated by the grouped object independently of the task demands or the respective attentional "set". Accordingly, our results are consistent with studies suggesting that, at least with central stimulus presentation, completion processes operate fairly automatically (Bakar et al., 2008; Wu et al., 2015; Poort et al., 2012). Of course, this does not rule out that it is necessary to attend to a given region to invoke the completion processes (see, e.g., Conci et al., 2018; Chen et al., 2019).

To summarize, we tracked the object construction process at the neural level and demonstrated that, while V1 is also contributing to the representation of a complete object, LOC is crucially involved in integrating Kanizsa-type illusory figures across graded, incremental steps of completion, irrespective of concurrent task demands. Thus, non-accidental figural properties in a visual scene are automatically extracted by object processing mechanisms in LOC, with right LO2 being more sensitive to global shape and left LOC (i.e., both LO1 and LO2) being implicated in the encoding of more detailed structures.

Author contributions

Siyi Chen: Conceptualization, Methodology, Software, Investigation, Formal analysis, Visualization, Writing- Original draft preparation, Project administration. **Ralph Weidner**: Supervision, Methodology, Software, Resources, Project administration, Writing- Reviewing and Editing. **Hang Zeng**: Investigation, Validation, Data curation. **Gereon R. Fink**: Resources, Writing- Reviewing and Editing. **Hermann J. Müller**: Conceptualization, Writing- Reviewing and Editing. **Markus Conci**: Supervision, Funding acquisition, Conceptualization, Methodology, Software, Writing- Reviewing and Editing.

Declaration of competing interest

The authors declare that they have no known competing financial interests or personal relationships that could have appeared to influence the work reported in this paper.

Acknowledgments

Appendix A. Supplementary data

Supplementary data to this article can be found online at https://doi.org/10.1016/j.neuroimage.2019.116426.

References

Awater, H., Kerlin, J.R., Evans, K.K., Tong, F., 2005. Cortical representation of space around the blind spot. J. Neurophysiol. 94, 3314–3324.

Bakar, A.A., Liu, L., Conci, M., Elliott, M.A., Ioannides, A.A., 2008. Visual field and task influence illusory figure responses. Hum. Brain Mapp. 29, 1313–1326.

Banton, T., Levi, D.M., 1992. The perceived strength of illusory contours. Percept. Psychophys. 52, 676–684.

Brainard, D.H., 1997. The psychophysics toolbox. Spat. Vis. 10, 433–436.

Chen, S., Glasauer, S., Müller, H.J., Conci, M., 2018a. Surface filling-in and contour interpolation contribute independently to Kanizsa figure formation. J. Exp. Psychol. Hum. Percept. Perform. 44, 1399–1413.

Chen, S., Nie, Q.-Y., Müller, H.J., Conci, M., 2019. Kanizsa-figure object completion gates selection in the attentional blink. Q. J. Exp. Psychol. 72, 1741–1755.

Chen, S., Töllner, T., Müller, H.J., Conci, M., 2018b. Object maintenance beyond their visible parts in working memory. J. Neurophysiol. 119, 347–355.

Conci, M., Böbel, E., Matthias, E., Keller, I., Müller, H.J., Finke, K., 2009. Preattentive surface and contour grouping in Kanizsa figures: evidence from parietal extinction. Neuropsychologia 47, 726–732.

Conci, M., Gramann, K., Müller, H.J., Elliott, M.A., 2006. Electrophysiological correlates of similarity-based interference during detection of visual forms. J. Cogn. Neurosci. 18, 880–888.

Conci, M., Groß, J., Keller, I., Müller, H.J., Finke, K., 2018. Attention as the "glue" for object integration in parietal extinction. Cortex 101, 60–72.

Conci, M., Müller, H.J., Elliott, M.A., 2007a. Closure of salient regions determines search for a collinear target configuration. Percept. Psychophys. 69, 32–47.

Conci, M., Müller, H.J., Elliott, M.A., 2007b. The contrasting impact of global and local object attributes on Kanizsa figure detection. Percept. Psychophys. 69, 1278–1294.

Cox, M.A., Schmid, M.C., Peters, A.J., Saunders, R.C., Leopold, D.A., Maier, A., 2013. Receptive field focus of visual area V4 neurons determines responses to illusory surfaces. Proc. Natl. Acad. Sci. U. S. A. 110, 17095–17100.

Erdfelder, E., Faul, F., Buchner, A., 1996. GPOWER: a general power analysis program. Behav. Res. Methods Instrum. Comput. 28, 1–11.

Ffytche, D.H., Zeki, S., 1996. Brain activity related to the perception of illusory contours. Neuroimage 3, 104–108.

Fink, G.R., Halligan, P.W., Marshall, J.C., Frith, C.D., Frackowiak, R.S., Dolan, R.J., 1996. Where in the brain does visual attention select the forest and the trees? Nature 382, 626–628.

Fink, G.R., Halligan, P.W., Marshall, J.C., Frith, C.D., Frackowiak, R.S., Dolan, R.J., 1997. Neural mechanisms involved in the processing of global and local aspects of hierarchically organized visual stimuli. Brain 120, 1779–1791.

Grabowska, A., Nowicka, A., Szymańska, O., Szatkowska, I., 2001. Subjective contour illusion: sex-related effect of unilateral brain damage. Neuroreport 12, 2289–2292.

Grossberg, S., 2000. The complementary brain: unifying brain dynamics and modularity. Trends Cogn. Sci. 4, 233–246.

Grossberg, S., Mingolla, E., 1985. Neural dynamics of form perception: boundary completion, illusory figures, and neon color spreading. Psychol. Rev. 92, 173–211.

Halgren, E., Mendola, J., Chong, C.D.R., Dale, A.M., 2003. Cortical activation to illusory shapes as measured with magnetoencephalography. Neuroimage 18, 1001–1009.

Han, S., Weaver, J.A., Murray, S.O., Kang, X., Yund, E.W., Woods, D.L., 2002. Hemispheric asymmetry in global/local processing: effects of stimulus position and spatial frequency. Neuroimage 17, 1290–1299.

Hirsch, J., DeLaPaz, R.L., Relkin, N.R., Victor, J., Kim, K., Li, T., Borden, P., Rubin, N., Shapley, R., 1995. Illusory contours activate specific regions in human visual cortex: evidence from functional magnetic resonance imaging. Proc. Natl. Acad. Sci. U. S. A. 92, 6469–6473.

Iidaka, T., Yamashita, K., Kashikura, K., Yonekura, Y., 2004. Spatial frequency of visual image modulates neural responses in the temporo-occipital lobe. An investigation with event-related fMRI. Cogn. Brain Res. 18, 196–204.

Kanizsa, G., 1955. Margini quasi-percettivi in campi con stimolazione omogenea. Riv. Psicol. 49, 7–30.

Kogo, N., Strecha, C., Van Gool, L., Wagemans, J., 2010. Surface construction by a 2-D differentiation–integration process: a neurocomputational model for perceived border ownership, depth, and lightness in Kanizsa figures. Psychol. Rev. 117, 406.

Kok, P., de Lange, F.P., 2014. Shape perception simultaneously up- and downregulates neural activity in the primary visual cortex. Curr. Biol. 24, 1531–1535.

Kourtzi, Z., Kanwisher, N., 2001. Representation of perceived object shape by the human lateral occipital complex. Science 293, 1506–1509.

Kubilius, J., Wagemans, J., Op de Beeck, H.P., 2011. Emergence of perceptual Gestalts in the human visual cortex: the case of the configural-superiority effect. Psychol. Sci. 22, 1296–1303.

Lamme, V.A., 1995. The neurophysiology of figure-ground segregation in primary visual cortex. J. Neurosci. 15, 1605–1615.

Larsson, J., Amunts, K., Gulyás, B., Malikovic, A., Zilles, K., Roland, P.E., 1999. Neuronal correlates of real and illusory contour perception: functional anatomy with PET. Eur. J. Neurosci. 11, 4024–4036.

Larsson, J., Heeger, D.J., 2006. Two retinotopic visual areas in human lateral occipital cortex. J. Neurosci. 26, 13128–13142. https://doi.org/10.1523/JNEUROSCI.1657-06.2006.

Lee, T.S., Nguyen, M., 2001. Dynamics of subjective contour formation in the early visual cortex. Proc. Natl. Acad. Sci. U. S. A. 98, 1907–1911.

Maertens, M., Pollmann, S., 2005. fMRI reveals a common neural substrate of illusory and real contours in V1 after perceptual learning. J. Cogn. Neurosci. 17, 1553–1564.

Maertens, M., Pollmann, S., 2007. Illusory contours do not pass through the blind spot. J. Cogn. Neurosci. 19, 91–101.

Maertens, M., Pollmann, S., Hanke, M., Mildner, T., Möller, H., 2008. Retinotopic activation in response to subjective contours in primary visual cortex. Front. Hum. Neurosci. 2, 2.

Marshall, J.C., Halligan, P.W., 1995. Seeing the forest but only half the trees? Nature 373, 521–523.

Mendola, J.D., Dale, A.M., Fischl, B., Liu, A.K., Tootell, R.B., 1999. The representation of illusory and real contours in human cortical visual areas revealed by functional magnetic resonance imaging. J. Neurosci. 19, 8560–8572.

Pelli, D.G., 1997. The VideoToolbox software for visual psychophysics: transforming numbers into movies. Spat. Vis. 10, 437–442.

Pessoa, L., Thompson, E., Noë, A., 1998. Filling-in is for finding out. Behav. Brain Sci. 21, 781–796.

Peterhans, E., von der Heydt, R., 1989. Mechanisms of contour perception in monkey visual cortex. II. Contours bridging gaps. J. Neurosci. 9, 1749–1763.

Peyrin, C., Baciu, M., Segebarth, C., Marendaz, C., 2004. Cerebral regions and hemispheric specialization for processing spatial frequencies during natural scene recognition. An event-related fMRI study. Neuroimage 23, 698–707.

Plewan, T., Weidner, R., Eickhoff, S.B., Fink, G.R., 2012. Ventral and dorsal stream interactions during the perception of the Müller-Lyer illusion: evidence derived from fMRI and dynamic causal modeling. J. Cogn. Neurosci. 24, 2015–2029.

Poort, J., Raudies, F., Wannig, A., Lamme, V.A.F., Neumann, H., Roelfsema, P.R., 2012. The role of attention in figure-ground segregation in areas V1 and V4 of the visual cortex. Neuron 75, 143–156.

Ritzl, A., Marshall, J.C., Weiss, P.H., Zafiris, O., Shah, N.J., Zilles, K., Fink, G.R., 2003. Functional anatomy and differential time courses of neural processing for explicit, inferred, and illusory contours. An event-related fMRI study. Neuroimage 19, 1567–1577.

Roelfsema, P.R., 2006. Cortical algorithms for perceptual grouping. Annu. Rev. Neurosci. 29, 203–227.

Rubin, N., Nakayama, K., Shapley, R., 1996. Enhanced perception of illusory contours in the lower versus upper visual hemifields. Science 271, 651–653.

Seghier, M., Dojat, M., Delon-Martin, C., Rubin, C., Warnking, J., Segebarth, C., Bullier, J., 2000. Moving illusory contours activate primary visual cortex: an fMRI study. Cerebr. Cortex 10, 663–670.

Smith, A.T., Singh, K.D., Williams, A.L., Greenlee, M.W., 2001. Estimating receptive field size from fMRI data in human striate and extrastriate visual cortex. Cereb. Cortex 11, 1182–1190.

Spillmann, L., Werner, J.S., 1996. Long-range interactions in visual perception. Trends Neurosci. 19, 428–434.

Stanley, D.A., Rubin, N., 2003. fMRI activation in response to illusory contours and salient regions in the human lateral occipital complex. Neuron 37, 323–331.

von der Heydt, R., Peterhans, E., Baumgartner, G., 1984. Illusory contours and cortical neuron responses. Science 224, 1260–1262.

Vuilleumier, P., Henson, R.N., Driver, J., Dolan, R.J., 2002. Multiple levels of visual object constancy revealed by event-related fMRI of repetition priming. Nat. Neurosci. 5, 491–499.

Wang, L., Mruczek, R.E.B., Arcaro, M.J., Kastner, S., 2015. Probabilistic maps of visual topography in human cortex. Cereb. Cortex 25, 3911–3931.

Wasserstein, J., Zappulla, R., Rosen, J., Gerstman, L., Rock, D., 1987. In search of closure: subjective contour illusions, Gestalt completion tests, and implications. Brain Cogn. 6, 1–14.

Weidner, R., Fink, G.R., 2007. The neural mechanisms underlying the Müller-Lyer illusion and its interaction with visuospatial judgments. Cerebr. Cortex 17, 878–884.

Wu, X., Zhou, L., Qian, C., Gan, L., Zhang, D., 2015. Attentional modulations of the early and later stages of the neural processing of visual completion. Sci. Rep. 5, 8346.

Zhaoping, L., 2003. V1 mechanisms and some figure–ground and border effects. J. Physiol. Paris 97, 503–515.